Thickness estimation of interface films formed on $Li_{1-x}CoO_2$ electrodes by hard X-ray photoelectron spectroscopy

Yu Takanashi[1], Yuki Orikasa[1], Masato Mogi[1], Masatsugu Oishi[1], Haruno Murayama[1], Kenji Sato[1], Hisao Yamashige[1], Daiko Takamatsu[1], Takahiro Fujimoto[1], Hajime Tanida[1], Hajime Arai[1], Toshiaki Ohta[2], Eiichiro Matsubara[3], Yoshiharu Uchimoto[4], Zempachi Ogumi[1]

[1]Center for Advanced Science and Innovation, Uji Campus Gokashou, 611-0011, Japan

[2]SR center, Ritsumeikan University, 1-1-1 Noji-Higashi, Kusatsu, Shiga 525-8577, Japan

[3]Department of Materials Science & Engineering, Kyoto University, Yoshida-Nihonmatsu-cho, Sakyo-ku, Kyoto 606-8501, Japan

[4]Graduate School of Human and Environmental Studies, Kyoto University, Yoshida-Nihonmatsu-cho, Sakyo-ku Kyoto 606-8501, Japan

Abstract

Solid electrolyte interface (SEI) films formed on $Li_{1-x}CoO_2$ electrodes were observed with hard X-ray photoelectron spectroscopy (HX-PES). This paper particularly focuses on film thickness estimation using HX-PES with theoretical calculation. The validity of the calculation was proven by experiments using model SEI films. The native film formed on a $LiCoO_2$ composite electrode was estimated to be LiF with its thickness of 5 nm. Formation of Co (II) species on top of $LiCoO_2$ was also indicated. Storage of the electrode at 60 °C brought about considerable film growth (30-40 nm) with carbonate compounds formation. SEI film changes during charging of the $LiCoO_2$ electrode were also examined. The main component in the film was deduced to be LiF or a kind of fluorite, with its thickness decreased during charging. The SEI formation mechanisms are also elucidated.

Keywords: Lithium ion batteries; SEI; HX-PES

1. Introduction

Lithium ion batteries (LIBs) are promising power sources for portable application such as mobile phones and laptop computers because of their high energy density. It is essential to improve the power capability and cycle performance of LIBs for new applications such as electric vehicles, load leveling and renewable energy accumulation. Recent reports on LIBs indicate that solid electrolyte interface (SEI) films on the positive electrode for LIBs are greatly responsible for limitation in power capability and cycle performance [1, 2]. It is thus important to detail the composition and the formation process of the SEI films on the positive electrode, which is not yet fully understood.

It has been indicated that the SEI is immediately formed after immersing electrodes into the organic electrolyte, generally accompanied with some electrolyte decomposition [3]. This SEI formation can restrict further electrolyte decomposition because of its electronically insulating nature, but cause interfacial resistance increases due to the limited ionic conductivity of the SEI films [4]. Lithium consumption with the SEI formation also results in battery performance degradation. The formation and the composition of the SEI film on the positive electrodes has been characterized with analytical methods such as infrared spectroscopy, Raman spectroscopy, X-ray photoelectron spectroscopy (XPS), scanning electron microscopy (SEM), nuclear magnetic resonance (NMR) spectroscopy, Auger electron spectroscopy (AES) and ellipsometry [5-24]. The component is generally a mixture of organic compounds such as carbonates and inorganic compounds such as Li_2O, Li_2CO_3 and LiF, which are similar to the SEI components on the negative electrodes. The thickness of the SEI film is generally considered to

be a few to several ten nanometers and increase with prolonged cycling/storage processes and high temperature exposure.

The XPS method is a powerful tool for observing the material surface and has been widely used for the SEI characterization, because of its surface sensitivity, element selectivity and ability to offer information on the chemical bonds around the target element. However, the applicability of this method to SEI analysis is unfortunately limited as the detection depth of XPS as laboratory facilities is generally less than 5 nm (see the following result for the detail), which is not enough to see the whole SEI film. Argon etching techniques have been often used to observe deeper parts of the film with laboratory XPS experiments, however, they are more or less destructive and native surface films are hardly evaluated. The AES method [23] can be also used for qualitative analysis, but the destructive etching is required to obtain the depth information. The ellipsometry [24] is useful for estimating the film thickness in a non-destructive way, but the kind of SEI components is unclear.

When the power of the X-ray source is sufficiently enhanced, the probe length of XPS can be large enough to observe the entire SEI film. By using the large probe length with hard X-ray photoelectron spectroscopy (or hard X-ray photoemission spectroscopy, HX-PES, HAX-PES), Shikano et al. have investigated the surface of positive electrode covered with SEI film and successfully obtained the information in tens of nanometer depth [21]. Therefore HX-PES is an effective method to investigate the film components as well as depth (film thickness) information of ten nanometer ranges.

In this study we examined the SEI film formed at the positive electrode surface with HX-PES using a synchrotron radiation source. Here we show a method for estimating the SEI film thickness with the HX-PES measurement, to the best of our knowledge, for the first time.

We describe how the SEI film thickness can be deduced with theoretical calculation, and show its validity with experimental results. Then we show and discuss the film growth during high temperature storage and the thickness changes during the charging process.

2. Experimental

The SEI film thickness was quantitatively obtained by calculating electronic signal attenuation due to inelastic scattering. The SEI component was first identified by qualitative analysis, and the electron free path was determined by the kind of atoms and density of the SEI components, then finally the effective escape depths of photoelectrons were used for SEI film thickness calculation. Effective escape depths of photoelectrons can be calculated using the theory shown in the literature [25]. The actual calculation was employed using NIST electron effective attenuation length database [26] with inputting the incident angle of the X-ray beam, the kinetic energy of the photoelectron E, and the asymmetry parameter β for the kind of photoelectron (such as $Co2p_{3/2}$) [27]. For each SEI component, the chemical composition, the number of the valence electrons contained in the unit cell N_v, the band gap E_g and the density d were used for the calculation. Examples of the parameters used for calculation are listed in Table 1. Thus obtained effective escape depth attenuation ratio was 1/e whereas the expected attenuation ratio was assumed to be 90 % of the emitted intensity where the photoelectron spectrum is no more observed. Assuming the Lambert-Beer's law, the spectrally escape depths were recalculated. The spectrally escape depth was calculated for the energy range between 50 to 2000 eV where the calculation program in the database works. The depth in higher energy ranges was obtained by extrapolating the values between 700 and 2000 eV, as it has been reported that the depth in this region is proportional to $\log(E)$ [31].

The validity of the depth calculation was examined as follows. In this validation process, a flat component on the substrate with a known thickness was necessary as a model electrode. The typical SEI components such as Li_2CO_3 and LiF were not available as flat films. Therefore, we fabricated flat thin film $LiCoO_2$ electrodes on nickel substrate with their thickness of 10 to 50 nm by using the pulsed laser deposition method, and attempted to use this $LiCoO_2$ film and the nickel substrate as a virtual SEI component and a surface covered electrode, respectively. The thickness of $LiCoO_2$ films was measured by a thickness profiler (Dektak 150, ULVAC). Ni $2p_{3/2}$ photoelectron spectra from below the $LiCoO_2$ film were measured and the results were compared with the calculated ones. The spectra were measured at BL47XU in SPring-8, Japan Synchrotron Radiation Research Institute, Hyogo Prefecture, Japan. The X-ray incident energy was 6 or 8 keV. The incident angle was 63 or 88 degrees.

The actual SEI formation at the positive electrode surface was examined as follows. A porous composite $LiCoO_2$ electrode was made of $LiCoO_2$ powder (Nichia Co.), acetylene black (Denki Kagaku Kogyo Co.) as a conductive agent and polyvinylidene difluoride (Kureha Co.) as a binder in a weight ratio of 8:1:1. The mixture was coated on an aluminum current collector with an electrode thickness of several ten μm. We made an electrochemical cell consisted of the $LiCoO_2$ electrode, lithium foil as a counter electrode, and an electrolyte solution of ethylene carbonate (EC) and ethylmethyl carbonate (EMC) (3:7 by volume) with 1 mol dm^{-3} $LiPF_6$ as a solute. Two cells were fabricated and kept at 25°C or 60 °C for a week before they were disassembled. The other cells were charged to a desired composition to form $Li_{1-x}CoO_2$ at a 27.4 mA g^{-1} rate (corresponding to 1/10 C for full delithiation) at 25 °C. The cell voltage after the relaxation period (> 3 h) was measured before they were disassembled. The cell was disassembled in an argon-filled glove box and the $LiCoO_2$ electrode was taken out, washed with dimethyl carbonate (DMC) to remove remaining $LiPF_6$ and dried prior to the XPS measurement.

All the samples were transferred to the vacuum chamber of the XPS apparatus via an argon-filled transfer vessel to avoid air exposure. The XPS signal intensity was normalized using C 1s signals (mostly that of acetylene black at 284 eV).

Here we focus on the interpretation of the Ni $2p_{3/2}$, Co $2p_{3/2}$, F 1s and C 1s spectra for clarity. The Li 1s, O 1s and P 2p spectra were also observed but the results are not shown in this paper because they provide little information due to the similar values in binding energy for various compounds and/or because the shifts/intensity are too small to be precisely determined, as it has been previously demonstrated [20].

3. Results and discussion

3.1 SEI thickness estimation

Figure 1 shows the calculated escape depth of Ni $2p_{3/2}$ photoelectrons from below the $LiCoO_2$ film. The depth for a laboratory XPS apparatus with typical photon energy of 1.5 keV is around a few nanometers, while that for the HX-PES with 6 or 8 keV is 19 or 24 nm, showing an expanded observation range for the latter. There is no essential difference in the calculated escape depth for the incident angles between 63 and 88 degrees. It has been reported that the depth can be controlled when the angle is extremely changed [21]. To prove the validity of the calculated escape depth, the intensity of the Ni $2p_{3/2}$ photoelectron from below the $LiCoO_2$ film was experimentally observed. The incident angle was fixed at 88 degree for the experiment shown in Fig. 2. Figure 2 (a) shows the result for the kinetic energy of 6 keV. The intensity for the 10 nm $LiCoO_2$ film is strong while it is nearly zero for the 20 nm $LiCoO_2$ film, indicating that the escape depth is around 20 nm. As shown in Fig. 2 (b), the intensity with the kinetic energy of 8 keV is strong for the 20 nm $LiCoO_2$ film but it is weak for the 30 nm $LiCoO_2$ film, suggesting that the escape depth is around 30 nm. Considering the roughness of the $LiCoO_2$ film

of a few nanometers, these results are in good agreement with the calculated values of 19 and 24 nm for 6 and 8 keV cases, respectively. Figure 3 represents the results with the incident angle of 63 and 88 degrees, in which the kinetic energy was fixed at 6 keV. The intensity fadeout for the 20 nm $LiCoO_2$ film was observed in both Figs. 3 (a) and (b), confirming the validity of the calculation. Figure 4 shows the calculated escape depth of Co $2p_{3/2}$ photoelectrons from below various SEI components with the incident angle of 88 degrees. It can be indicated that the depth values are similar to each other but the photoelectrons easily penetrate thorough light SEI components such as LiF. Using these data, the escape depth of the photoelectron from the electrode element (mostly transition metals) can be correlated with the SEI film thickness. Accordingly, the SEI film thickness can be quantitatively evaluated by using theoretical calculation and experimental observation for the HX-PES measurements. The incident angle of 88 degrees and the kinetic energy of 6 keV were used for further experiments for the SEI evaluation.

3.2 SEI Growth in electrolyte storage

The Co $2p_{3/2}$ and the F 1s photoelectron spectra of the composite $LiCoO_2$ electrodes are shown in Figs. 5 and 6, respectively. Both figures contain the spectra before and after the electrolyte soaking process at 25 °C. In Fig. 5, there is a peak intensity decrease with the electrolyte soaking process, which is indicative of the SEI formation on the $LiCoO_2$ electrode. Figure 6 shows that a LiF peak is observed at 685 eV in addition to a PVDF peak at 687 eV [21]. The absence of peaks in the P 2p spectrum (not shown) suggests that $LiPF_6$ was removed with the DMC washing process. There was essentially no change in the C 1s spectrum (not shown) between before and after the electrolyte soaking, therefore, we attributed the intensity decrease

in Fig. 5 to the LiF formation. We estimated this SEI thickness to be 5.3 nm, using the procedure shown in the experimental section.

In Fig. 5, a small peak shift to lower energy levels is also observed with the soaking process, indicative of surface cobalt reduction. This implies that the LiF formation accompanied with $LiCoO_2$ related charge transfer reactions. The LiF formation reaction, which occurs at high temperatures such as 70 °C, has been previously deduced as follows [2].

$$LiPF_6 \rightarrow LiF + PF_5 \quad (1)$$

However, this simple acid-base reaction is free from any charge transfer process, and thus hardly explains the surface cobalt reduction. As organic electrolyte solutions consisted of $LiPF_6$ inevitably contained some water of at least in a ppm level, it is suggested that $LiPF_6$ decomposition shown in reaction (2) occurs and then the $LiCoO_2$ disproportionation reaction shown in reaction (3) occurs with hydrogen fluoride HF [13].

$$2LiPF_6 + 5H_2O \rightarrow 2LiF + 10HF + P_2O_5 \quad (2)$$

$$4LiCoO_2 + 4HF \rightarrow CoO_2 + Co_3O_4 + 4LiF + 2H_2O \quad (3)$$

Thus formed CoO_2 should be unstable and react with organic solvents. For example, reaction (4) represents EC oxidation. A similar reaction should occur to EMC as well.

$$CoO_2 + 1/5C_3H_4O_3 \rightarrow CoO + 3/5CO_2 + 2/5H_2O \quad (4)$$

As a result, such low valence cobalt species are formed until the charge transfer reactions (3) and (4) are hindered by the insulating SEI film formation The existence of low valence nickel compounds like NiO has been suggested for nickel-based positive electrode materials [13, 21].

Figure 7 shows the Co $2p_{3/2}$ spectra of the composite $LiCoO_2$ electrodes after storage at 25 and 60 °C. There was nearly no spectrum observed for the storage at 60 °C. For the sample stored at 60 °C, the formation of CH_3OCO_2Li at 287 eV and Li_2CO_3 at 290 eV [9] was deduced from the C 1s spectra shown in Fig. 8. As LiF was also contained in the SEI film, we were not

able to identify the main SEI components. Nevertheless, the individually estimated SEI thickness for LiF, and CH_3OCO_2Li, Li_2CO_3 are 38, 29 and 27 nm, which are around 30-40 nm. These values are useful for a semi-quantitative analysis. It should be also noted that such thick films are hardly observed with the laboratory XPS apparatus. The formation of CH_3OCO_2Li and Li_2CO_3 can be attributed to the decomposition of EMC and EC. Both LiF [19] and these carbonate related compounds [10, 22] reportedly form in the SEI film at elevated temperatures.

It is accordingly concluded that the method presented here is useful to evaluate the SEI thickness at least semi-quantitatively and can be applied to observe the SEI formation under various conditions.

3.3 SEI changes during lithium extraction

The SEI film changes during lithium extraction (delithiation) from the $LiCoO_2$ electrode were observed at 25 °C. The nominal composition of each sample as well as its open circuit voltage before the cell disassembly is plotted in Fig. 9. The voltage increased with the delithiation process and the close circuit voltage reached 5.0 V when fully delithiated. The open circuit voltage for "CoO_2" was 4.51 V, though the current efficiency for the delithiation process may be less than unity at the end of the charging process. Figure 10 shows the Co $2p_{3/2}$ spectra for the delithiated samples. The peak energy shifted to lower values at the early stage of delithiation, suggesting that surface cobalt species were reduced, despite that the average oxidation state of cobalt should be larger than +3 during the delithiation process of the $LiCoO_2$ electrode. Again, surface cobalt species such as CoO and Co_3O_4 seemed to be formed during this process. The Co $2p_{3/2}$ spectra were unchanged during further delithiation for $0.2 \leq x \leq 1.0$ in $Li_{1-x}CoO_2$. It was observed that the intensity of the Co $2p_{3/2}$ spectra were nearly unchanged. Figure 11 shows the F 1s spectra for the delithiated samples. The peak energy shifted to lower

values (685 to 684 eV) and the intensity gradually decreased during the delithiation process. The C1s spectra in Fig. 12 indicate that there was a little increase in peak intensity at 288 eV and 290 eV, which respectively correspond to alkyl carbonate $ROCO_2Li$ and Li_2CO_3 [9]. However, these small changes of the C 1s spectra cannot explain the large intensity decrease observed in F 1s spectra in Fig. 11. Therefore, we suggest that the intensity decrease observed in F 1s spectra is mainly ascribed to a film thickness decrease. Assuming that this film is LiF, the thickness change is plotted in Fig. 13. The thickness was more than 5 nm in the beginning, but finally reached a very small value of around 1 nm. Such LiF film thickness decrease during charging has barely been reported. If the LiF particle is aggregated to form large grain size, the apparent intensity would decrease [10]. Other possible reasons are fluoride-oxide conversion and removal of the film with gas evolution from the electrode surface during the charging process. The laboratory XPS observation suggests LiF intensity increase during charging up to 4.2 V [20], but this may not contradict the result in this study obtained with HX-PES. The Li_2CO_3 film thickness decrease during charging has been reported [22]. As to the peak energy shift observed in Fig. 11, it seems the fluorine related bond nature changes from covalent to ionic. This reminds us compounds such as CoF_2 or CoOF. The formation of CoF_2 can occur by the reaction of CoO and HF as shown in reaction (5). The formation of CoOF could also occur by the reaction of CoO, CoO_2 and HF as shown in reaction (6).

$$CoO+2HF\rightarrow CoF_2+H_2O \quad (5)$$

$$CoO+CoO_2+2HF\rightarrow 2CoOF+H_2O \quad (6)$$

Though the assignment of the peak at 684 eV is unclear at the moment, it has been reported that a XPS peak of around 684 keV is observed in the F 1s spectra for a $LiCoO_2$ electrode in contact with an electrolyte solution containing Co^{2+} [32]. Further detailed study is needed to clarify the SEI change during the charge-discharge process. Nevertheless the method described here can be

applied for examining many cases including solvent/solute composition effects, SEI depth profile observation and electrode potential and temperature effects, and will give fruitful information on the nature and formation process of the SEI film. The technique described in this paper can be also applied to estimate the thickness of other films, such as coated films on the electrode materials.

Conclusion

Hard X-ray photoelectron spectroscopy (HX-PES) is shown to be useful for observing solid electrolyte interface (SEI) films. The film thickness can be estimated by using theoretical calculation and HX-PES experiments. The validity of the calculation can be proven by experiments using model SEI films. When a $LiCoO_2$ composite electrode is immersed in an electrolyte solution containing $LiPF_6$ at 25 °C, the SEI film is estimated to be LiF with its thickness of 5 nm, accompanied with the formation of Co (II) species on top of $LiCoO_2$. The SEI film grows to 30-40 nm when such electrodes are stored at 60 °C, which should be detrimental to the cell performance. The content of a fluoride-related component in the SEI film decreases during charging of the $LiCoO_2$ electrode, which could be ascribed to fluoride-oxide conversion or removal of the film with gas evolution from the electrode surface.

Acknowledgment

The authors also acknowledge New Energy and Industrial Technology Department Organization (NEDO) for supporting R&D Initiative for Scientific Innovation on New Generation Batteries (RISING) Project where this study was employed.

References

1. K. Amine, C.H. Chen, J. Liu, M. Hammond, A. Jansen, D. Dees, I. Bloom, D. Vissers and G. Henriksen, *J. Power Sources* 97/98 (2001) 684.

2. X. Zhang, P.N. Ross, R. Kostecki, F. Kong, S. Sloop, J.B. Kerr, K. Striebel, E.J. Cairns and F. McLarnon, *J. Electrochem. Soc*. 148 (2001) A463.

3. E. Peled and H. Yamin, *J. Electrochem. Soc.* 126 (1979) 2047.

4. M.G.S.R. Thomas, P. Bruce and J.B. Goodenough, *J. Electrochem. Soc.* 132 (1985) 1521.

5. D. Aurbach, M.D. Levi, E. D.Levi, H. Teller, B. Markovsky, G. Salitra, U. Heider and L. Heider, *J. Electrochem. Soc.* 145 (1998) 3024.

6. D. Aurbach, K. Gamolsky, B. Markovsky, G. Salitra, Y. Gofer, U. Heider, R. Oesten and M. Schmidt, *J. Electrochem. Soc.* 147 (2000) 1322.

7. T. Uchiyama, M. Nishizawa, T. Itoh and I. Uchida, *J. Electrochem. Soc.* 147 (2000) 2057.

8. Y. Wang, X. Guo, S. Greenbaum, J. Liu and K. Amine, *Electrochem Solid-State Lett.* 4 (2001) A68.

9. T. Eriksson, A.M. Andersson, A.G. Bishop, C. Gejke, T. Gustafsson and J.O. Thomas, *J. Electrochem. Soc.* 149 (2002) A69.

10. A.M. Andersson, D.P. Abraham, R. Haasch, S. MacLaren, J. Liu, K. Amine, *J. Electrochem. Soc.* 149 (2002) A1358.

11. M. Balasubramanian, H.S. Lee, X. Sun, X.Q. Yang, A.R. Moodenbaugh, J. McBreen, D.A. Fischer and Z. Fu, *Electrochem .Solid-State Lett.* 5 (2002) A22.

12. D. Aurbach, B. Markovsky, A. Rodkin, M. Cojocaru, E. Levi and H.J. Kim, *Electrochimica Acta* 47 (2002) 1899.

13. D.P. Abraham, R.D. Twesten, M. Balasubramanian, J. Kropf, D. Fischer, J. McBreen, I. Petrov and K. Amine, *J. Electrochem. Soc.* 150 (2003) A1450.

14. B. Markovsky, A. Rodkin, Y.S. Cohen, O. Palchik, E. Levi and D. Aurbach, *J. Power Sources* 119/121 (2003) 504.

15. G.V. Zhuang, G.Y. Chen, J. Shim, X.Y. Song, P.N. Ross and T.J. Richardson, *J. Power Sources* 134 (2004) 293.

16. M. Menetrier, C. Vaysse, L. Croguennec, C. Delmas, C. Jordy, F. Bonhomm and P. Biensan, *Electrochem Solid-State Lett.* 7 (2004) A140.

17. A. Wursig, H. Buqa, M. Holzapfel, F. Krumeich and P. Novak, *Electrochem Solid-State Lett.* 8 (2005) A34.

18. B.M. Meyer, N. Leifer, S. Sakamoto, S.G. Greenbaum and P. Grey, *Electrochem Solid-State Lett.* 8 (2005) A145.

19. D. Aurbach, B. Markovsky, G. Salitra, E. Markevich, Y. Talyossef, M. Koltypin, L. Nazar, B. Ellis and D. Kovacheva, *J. Power Sources* 165 (2007) 491.

20. R.Dedryvère, H. Martinez,S. Leroy,D. Lemordant, F.Bonhomme, P.Biensan and D. Gonbeau, *J. Power Sources* 174 (2007) 462.
21. M. Shikano, H. Kobayashi, S. Koike, H. Sakaebe, E. Ikenaga, K. Kobayashi and K. Tatsumi, *J. Power Sources* 174 (2007) 795.
22. M.K. Rahman and Y. Saito, *J. Power Sources* 174 (2007) 889.
23. K. Abe, H. Yoshitake, T. Kitakura, T. Hattori, H. Wang and M. Yoshio, *Electrochimica Acta* 49 (2004) 4613.
24. J. Lei, L. Li, R. Kostecki, R. Muller and F. *J. Electrochem. Soc*. 152 (2005) A774.
25. M.Sacchi, F.Offi, P.Torelli, A.Fondacaro, C.Spezzani, M.Cautero, G.Cautero, S.Huotari, M.Grioni, R.Delaunay, M.Fabrizioli, G.Vanko, G.Monaco, G.Paolicelli, G.Stefani, G.Panaccione, *Phys.Rev.B*71 (2005)
26. C.J.Powell, A.Jablonski, *NIST Electron Effective-Attenuation-Length Database, Version 1.3, SRD 82, National Instutute of Standards and Technology, Gaithersburg, MD* (2011)
27. I.M.Band, Y.I.Kharitonov, M.B.Trzhaskovskaya, *At. Data Nucl. Data Tables*,23 (1979) 443.
28. J.M. Rosolen, F.Decker, *J. Electroanal. Chem.* 501 (2001) 253.
29. .Schlaf,B.A.Parkinson,P.A.Lee,K.W.Nebesny,G.Jabbour,B.Kippelen,N.Peyghambarian,R.Armstrong, *J. Appl. Phys* 84 (1998) 6729.
30. Y.Duan, D.C.Sorescu, *Phys. Rev. B* 79 (2009) 014301.
31. C.J. Powell, A.Jablonski, *J. Phys. Chem. Ref. Data*, 28 (1999) 19.
32. B. Markovsky, A. Rodkin, G. Salitra,Y. Talyosef, D. Aurbach and H.J. Kim, *J. Electrochem. Soc.* 151 (2004) A1068.

Figure captions

Figure 1 Calculated escape depth of Ni $2p_{3/2}$ photoelectrons from below $LiCoO_2$ film. Open circles and filled squares indicate data with X-ray incident angles of 63 and 88 degrees, respectively.

Figure 2 Ni $2p_{3/2}$ photoelectron spectra of metallic nickel from below $LiCoO_2$ film with kinetic energy of (a) 6 keV and (b) 8 keV. The incident angle is at 88 degree. Bold solid lines, bold broken lines, thin solid lines and thin broken lines indicate data with $LiCoO_2$ film thickness of 10, 20, 30 and 50 nm, respectively.

Figure 3 Ni $2p_{3/2}$ photoelectron spectra of metallic nickel from below $LiCoO_2$ film with X-ray incident angle of 88 (a) and 63 (b) degrees. The kinetic energy is 6 keV. Bold lines, bold broken lines, thin lines and thin broken lines indicate data with $LiCoO_2$ film thickness of 10, 20, 30 and 50 nm, respectively.

Figure 4 Calculated escape depth of Co $2p_{3/2}$ photoelectrons from below LiF (triangles), Li_2CO_3 (circles) and CH_3OCO_2Li (squares) with X-ray incident angle of 88 degrees.

Figure 5 Co $2p_{3/2}$ photoelectron spectra of composite $LiCoO_2$ electrodes spectra before (solid line) and after (broken line) electrolyte soaking process at 25 °C.

Figure 6 F 1s photoelectron spectra of composite $LiCoO_2$ electrodes spectra before (solid line) and after (broken line) electrolyte soaking process at 25 °C.

Figure 7 Co $2p_{3/2}$ photoelectron spectra of composite $LiCoO_2$ electrodes after storage at 25 (solid line) and 60 °C (broken line).

Figure 8 C 1s photoelectron spectra of composite $LiCoO_2$ electrodes after storage at 25 (solid line) and 60 °C (broken line).

Figure 9 Closed (filled squares) and open (open circuits) voltage of $Li_{1-x}CoO_2$ / Li cell during charging at 25 °C. The symbols indicate the nominal composition where the XPS measurements were employed.

Figure 10 Co $2p_{3/2}$ photoelectron spectra of composite $Li_{1-x}CoO_2$ electrode. Bold solid line, bold broken line, thin solid line, thin broken line and dotted line indicate spectra for x=0.0, x=0.1, x=0.4, x=0.8 and x=1.0, respectively.

Figure 11 F 1s photoelectron spectra of composite $Li_{1-x}CoO_2$ electrode. (a) Solid line, broken line, dotted line and gray line indicate spectra for x=0.0, x=0.1 and x=0.4, respectively. (b) Solid line, broken line and dotted line indicate spectra for x=0.6, x=0.8 and x=1.0, respectively.

Figure 12 C 1s photoelectron spectra of composite $Li_{1-x}CoO_2$ electrode. Solid line, broken line and dotted line indicate spectra for x=0.0, x=0.4 and x=1.0, respectively.

Figure 13 Estimated LiF film thickness formed on composite $Li_{1-x}CoO_2$ electrode.

Table 1 Parameters used for calculating effective escape depth

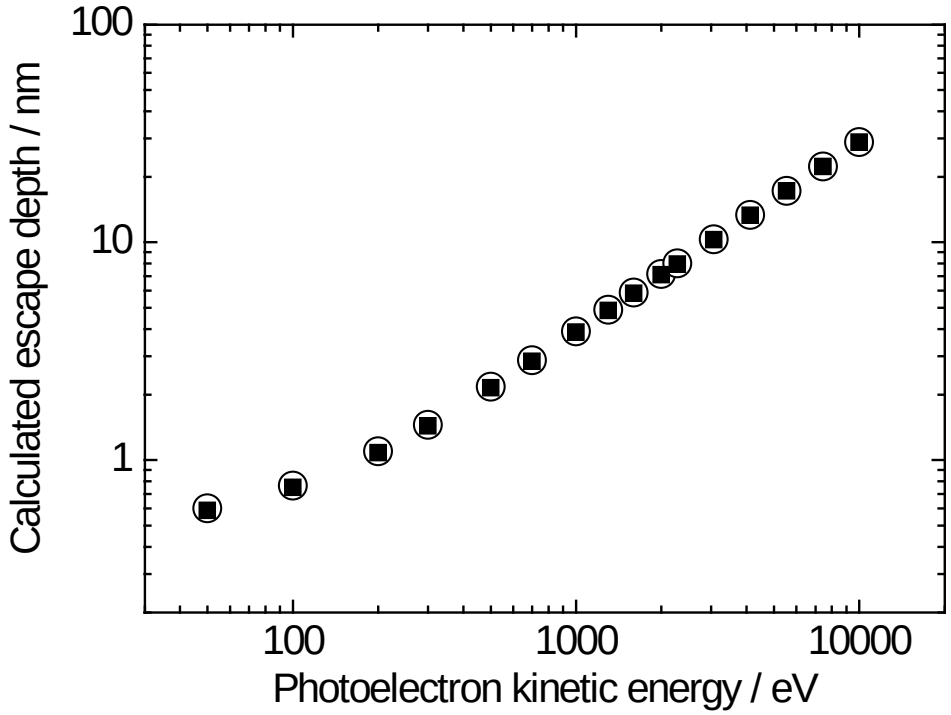
100
10
1
Calculated escape depth / nm
100
1000
10000
Photoelectron kinetic energy / eV

Figure. 1

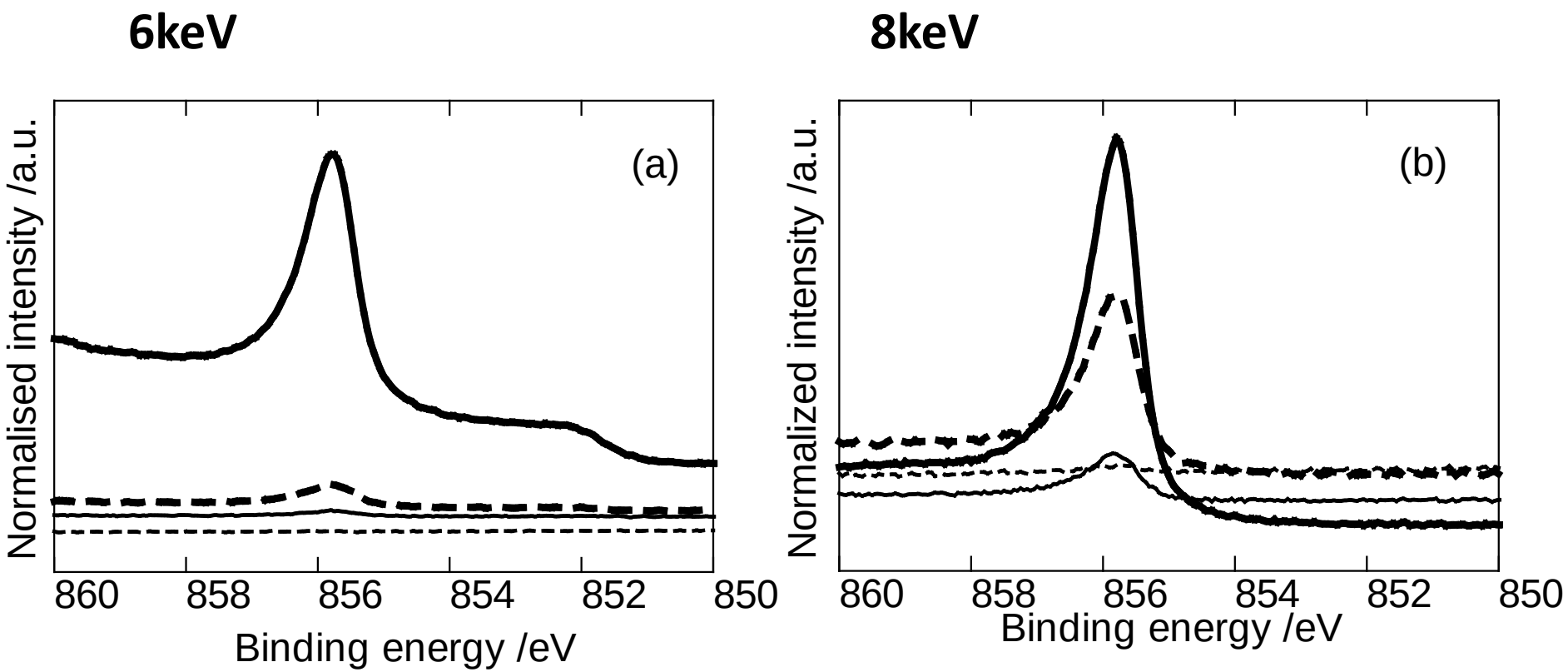
6keV
8keV
(a)
(b)
Normalised intensity /a.u.
Normalized intensity /a.u.
860
858
856
854
852
850
Binding energy /eV

Figure. 2

88deg

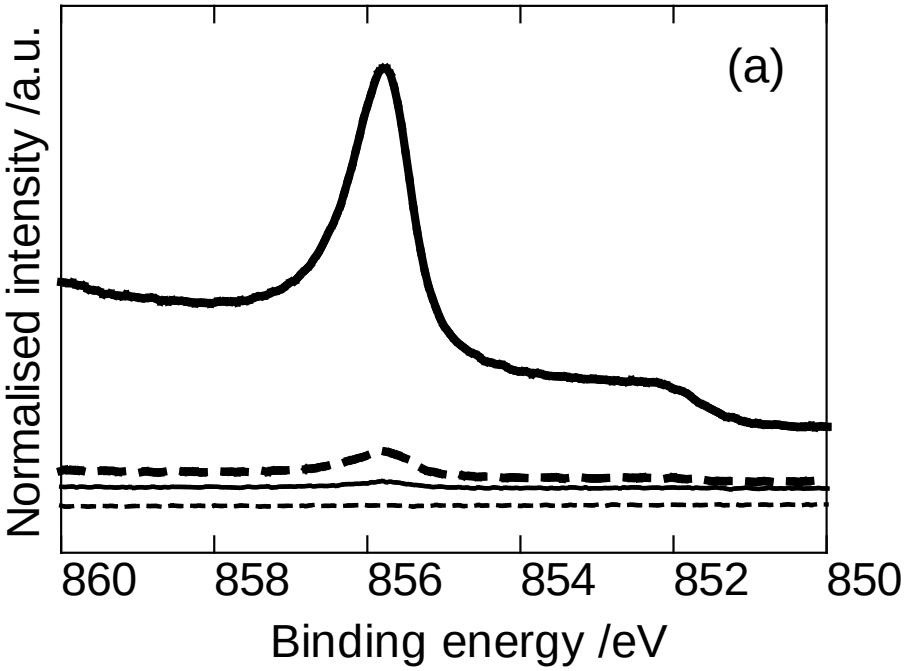

63deg

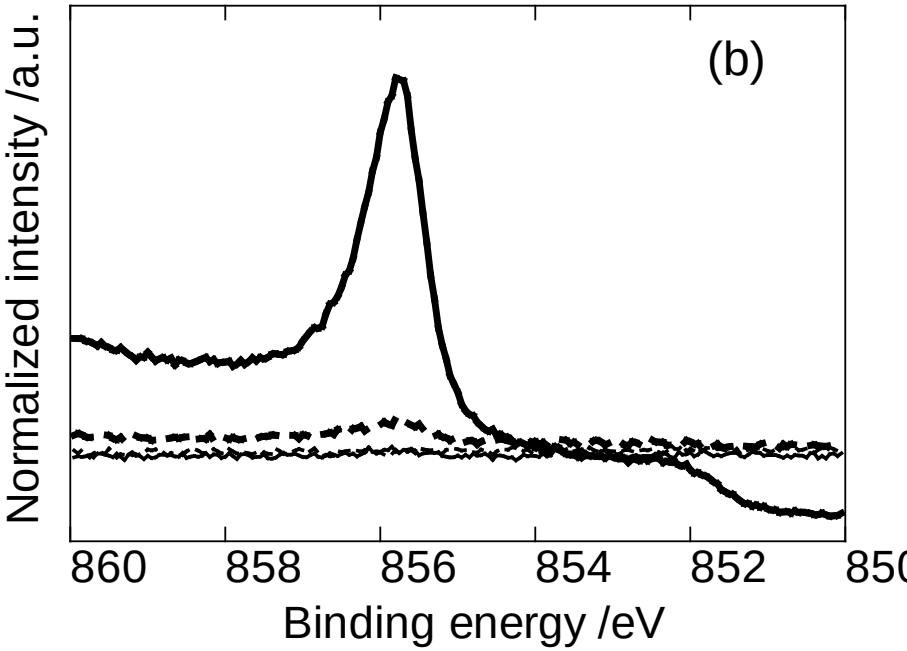

Figure. 3

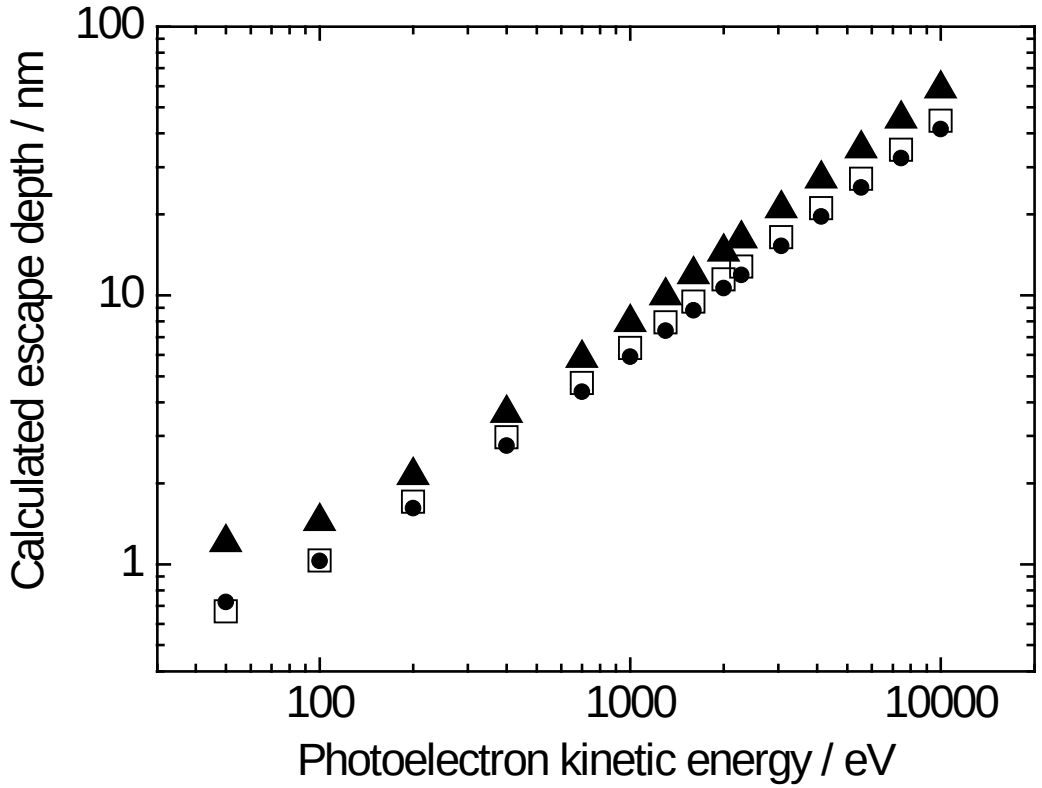
100
10
1
Calculated escape depth / nm
100
1000
10000
Photoelectron kinetic energy / eV

Figure. 4

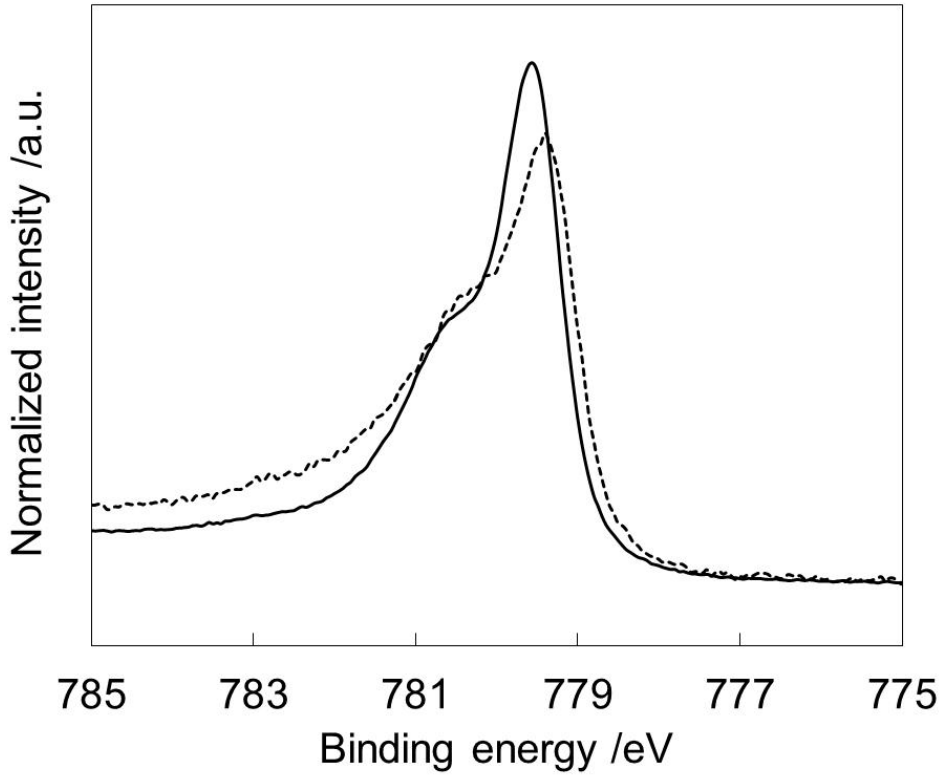
Normalized intensity /a.u.
785
783
781
779
777
775
Binding energy /eV

Figure. 5

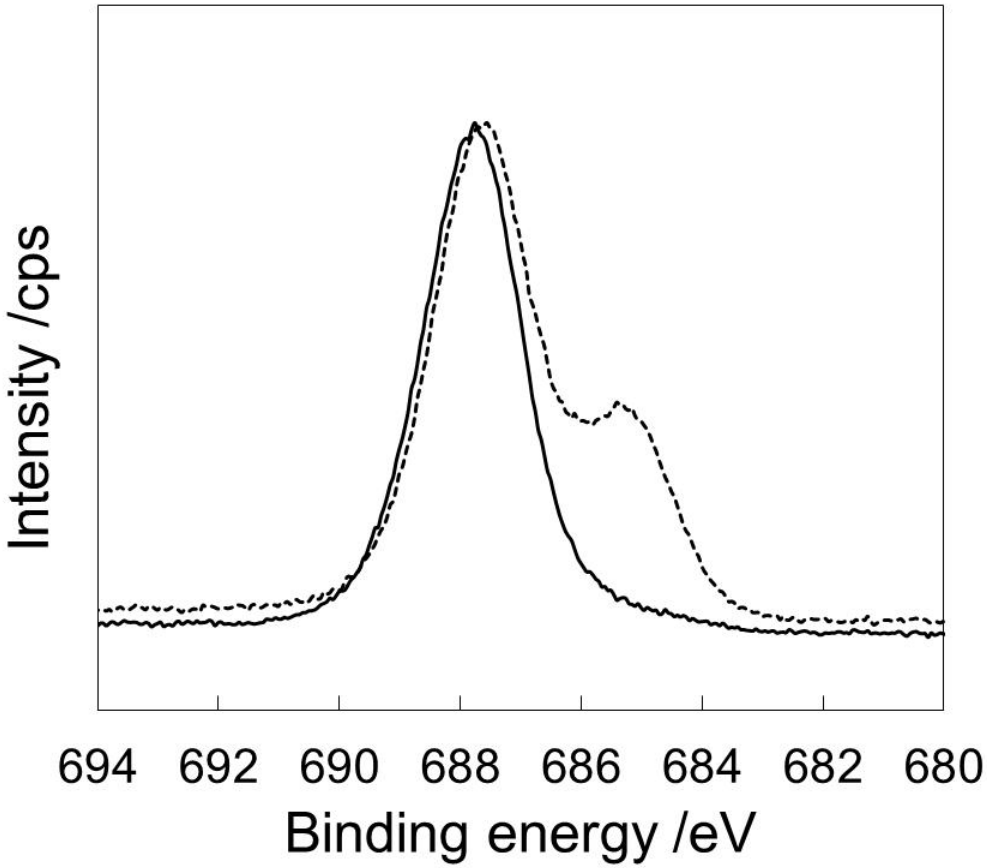
Intensity /cps
694
692
690
688
686
684
682
680
Binding energy /eV

Figure. 6

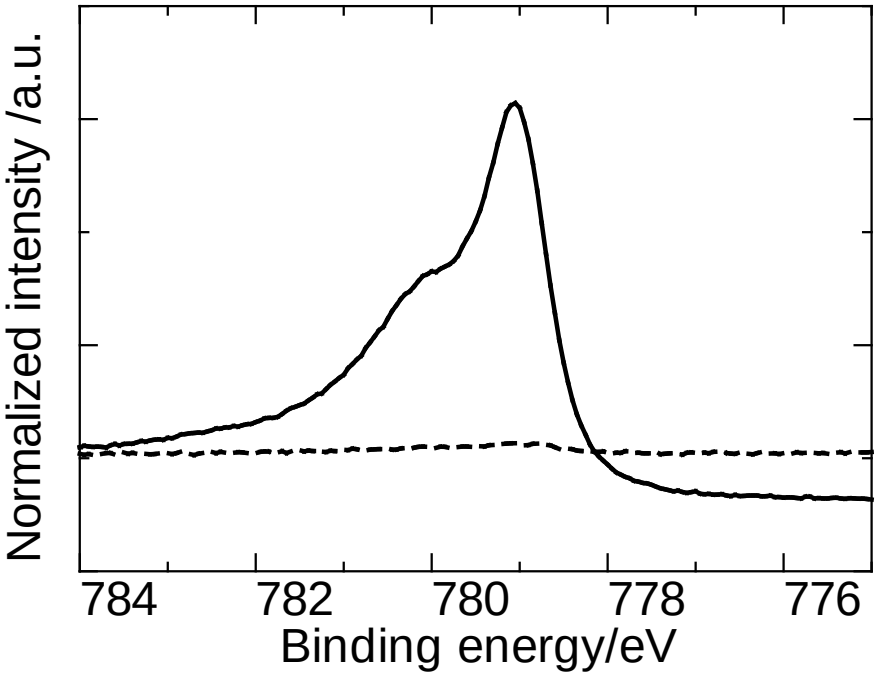
Normalized intensity /a.u.
784
782
780
778
776
Binding energy/eV

Figure. 7

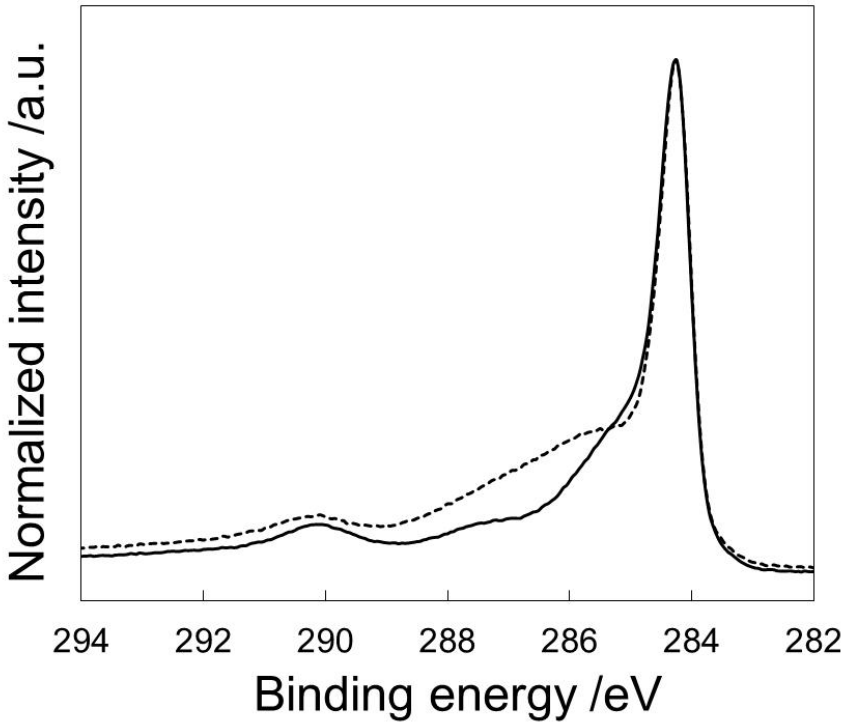
Normalized intensity /a.u.
294
292
290
288
286
284
282
Binding energy /eV

Figure. 8

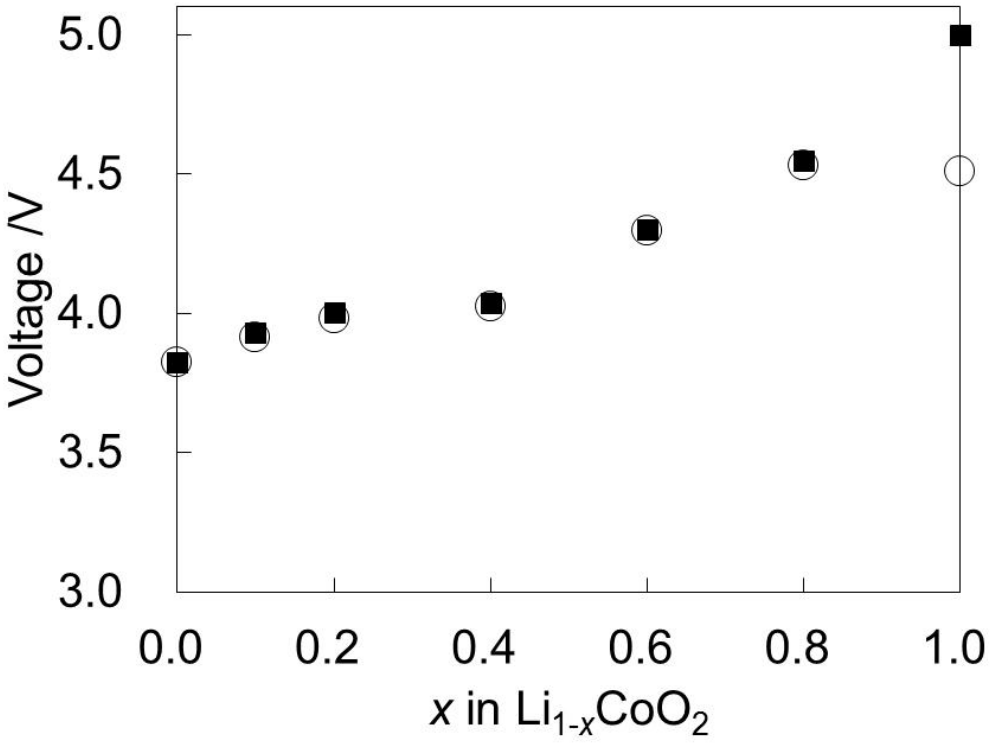

Figure. 9

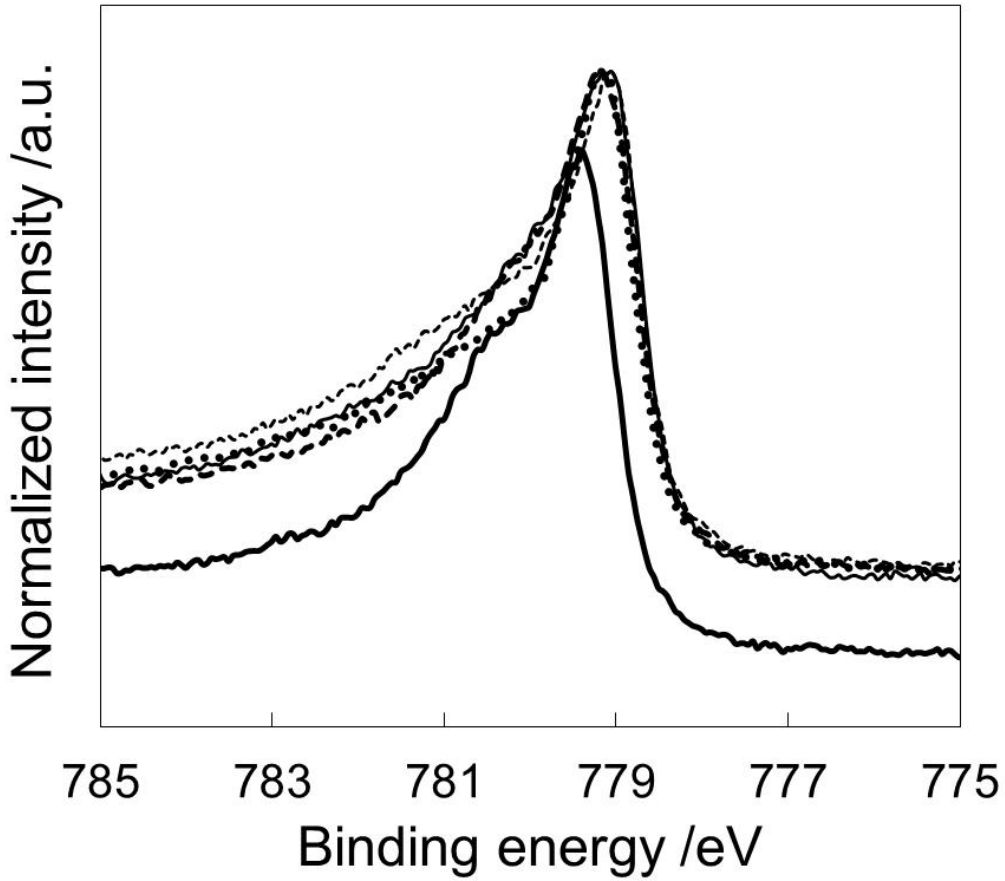
Normalized intensity /a.u.
785
783
781
779
777
775
Binding energy /eV

Figure. 10

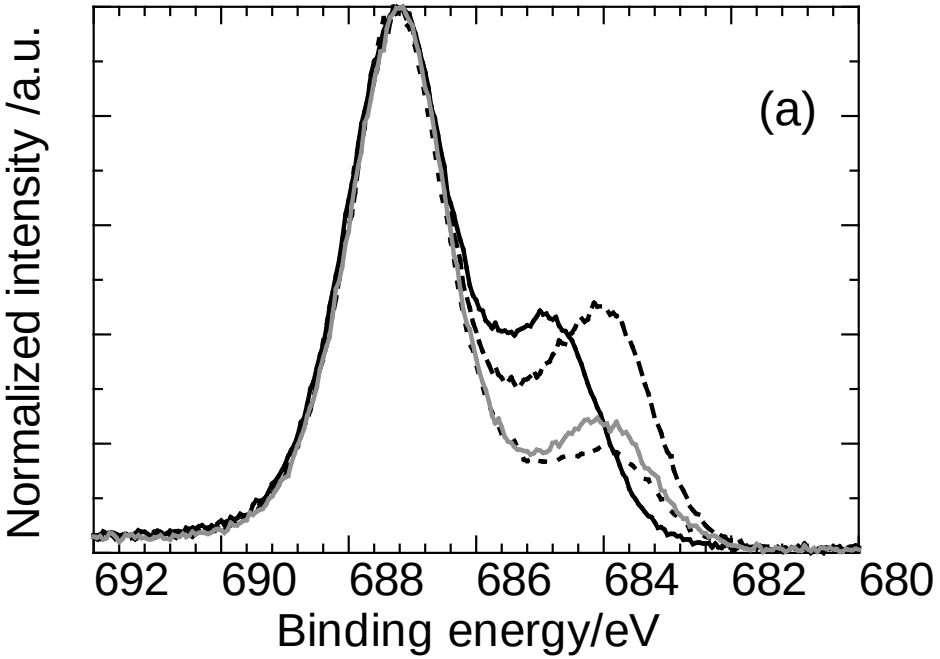
Normalized intensity /a.u.
(a)
692
690
688
686
684
682
680
Binding energy/eV

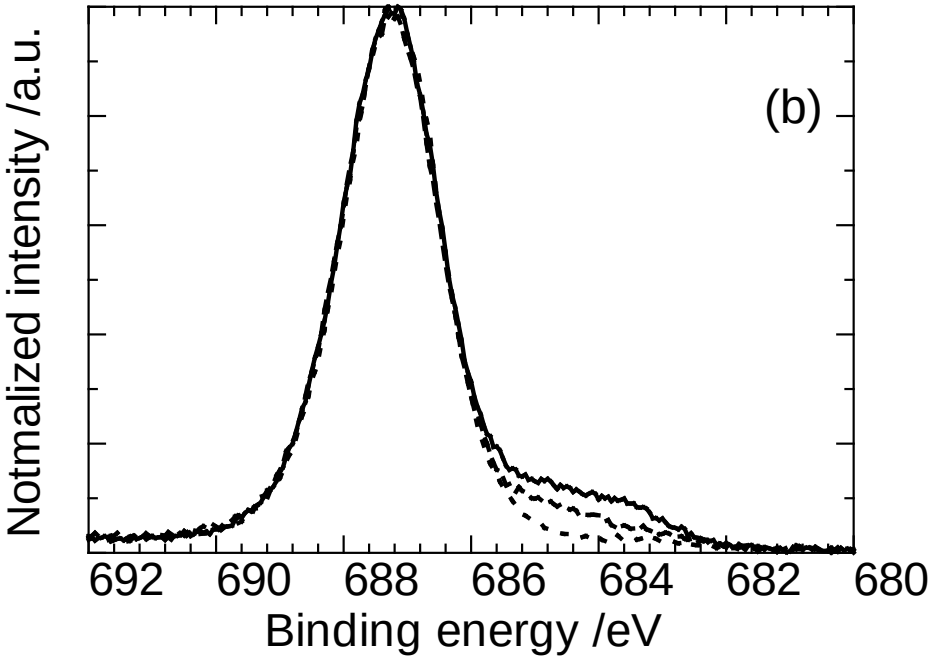
Notmalized intensity /a.u.
(b)
692
690
688
686
684
682
680
Binding energy /eV

Figure. 11

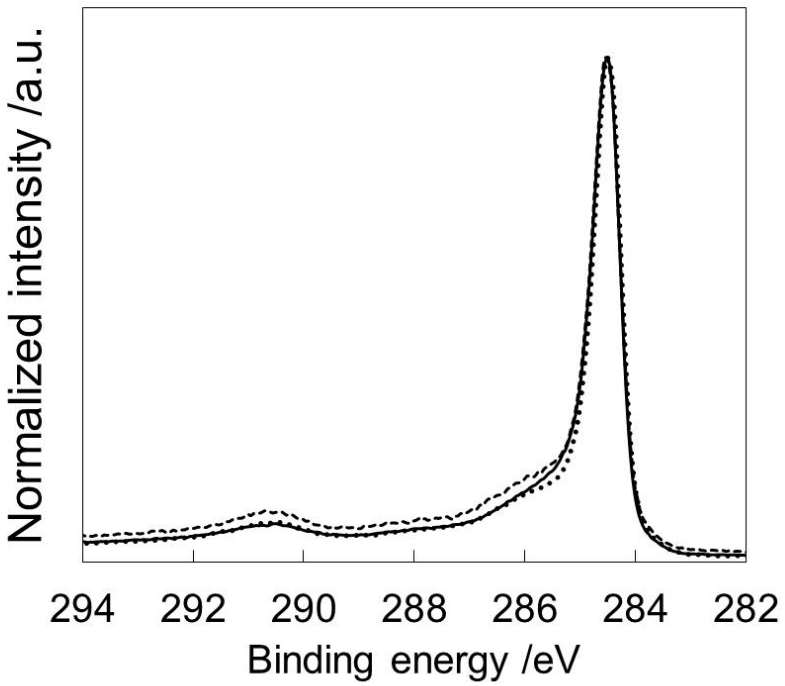

Figure. 12

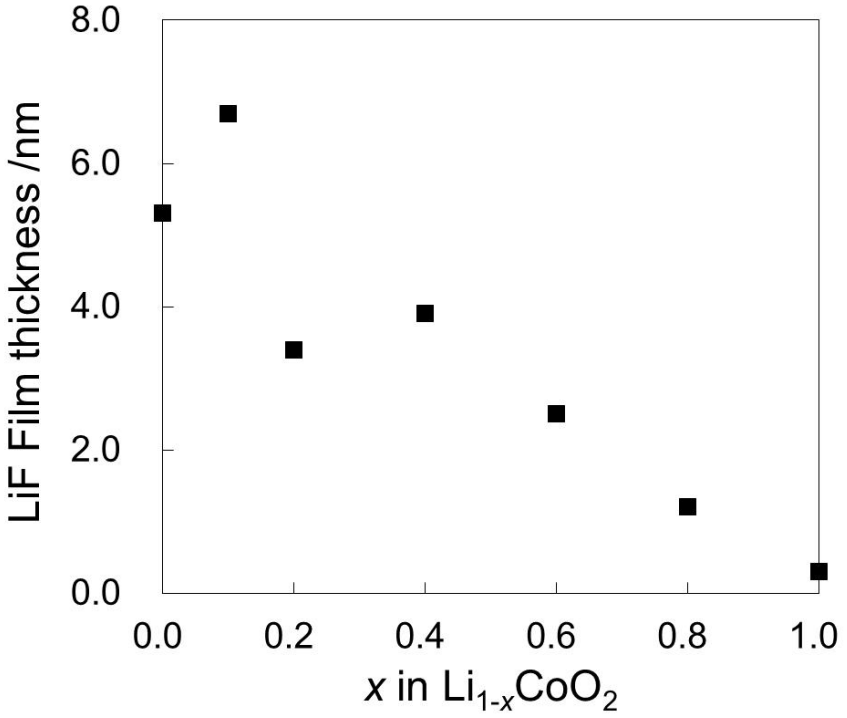

Figure. 13

Table 1

Photoelectron	SEI component	N_v	E_g / eV	d / g cm^{-3}	Reference
Ni $2p_{3/2}$	$LiCoO_2$	22	2.5	5.03	[26]
Co $2p_{3/2}$	LiF	8	14	2.62	[27]
Co $2p_{3/2}$	Li_2CO_3	24	5.1	2.1	[28]

Photoelectron	SEI component	N_v	E_g / eV	d / g cm^{-3}	Reference
Ni $2p_{3/2}$	$LiCoO_2$	22	2.5	5.03	[26]
Co $2p_{3/2}$	LiF	8	14	2.62	[27]
Co $2p_{3/2}$	Li_2CO_3	24	5.1	2.1	[28]

Photoelectron	SEI component	N_v	E_g / eV	d / g cm^{-3}	Reference
Ni $2p_{3/2}$	$LiCoO_2$	22	2.5	5.03	[26]
Co $2p_{3/2}$	LiF	8	14	2.62	[27]
Co $2p_{3/2}$	Li_2CO_3	24	5.1	2.1	[28]